



Tafenoquine and its derivatives as inhibitors for the severe acute respiratory syndrome coronavirus 2

Received for publication, July 27, 2021, and in revised form, January 20, 2022. Published, Papers in Press, January 29, 2022.
<https://doi.org/10.1016/j.jbc.2022.101658>

Yeh Chen^{1,2,3,*,#}, Wen-Hao Yang^{2,3,4,5,#}, Hsiao-Fan Chen^{4,#}, Li-Min Huang^{6,#}, Jing-Yan Gao^{2,7,#}, Cheng-Wen Lin^{8,9}, Yu-Chuan Wang¹, Chia-Shin Yang¹, Yi-Liang Liu¹⁰, Mei-Hui Hou¹, Chia-Ling Tsai¹, Yi-Zhen Chou¹, Bao-Yue Huang⁴, Chian-Fang Hung⁴, Yu-Lin Hung¹¹, Wei-Jan Wang^{3,12}, Wen-Chi Su⁴, Vathan Kumar², Yu-Chieh Wu⁷, Shih-Wei Chao², Chih-Shiang Chang^{2,7}, Jin-Shing Chen¹³, Yu-Ping Chiang⁶, Der-Yang Cho^{4,14}, Long-Bin Jeng^{15,16}, Chang-Hai Tsai^{15,17}, and Mien-Chie Hung^{2,3,4,5,18,*}

From the ¹Institute of New Drug Development, ²Drug Development Center, ³Research Center for Cancer Biology, ⁴Graduate Institute of Biomedical Sciences, and ⁵Center for Molecular Medicine, China Medical University, Taichung, Taiwan; ⁶Department of Pediatrics, College of Medicine, National Taiwan University, Taipei, Taiwan; ⁷School of pharmacy, College of Pharmacy, and ⁸Department of Medical Laboratory Science and Biotechnology, China Medical University, Taichung, Taiwan; ⁹Department of Medical Laboratory Science and Biotechnology, Asia University, Taichung, Taiwan; ¹⁰Department of Life Sciences, National Chung Hsing University, Taichung, Taiwan; ¹¹Program of Digital Health Innovation, and ¹²Department of Biological Science and Technology, China Medical University, Taichung, Taiwan; ¹³Department of Surgery, College of Medicine, National Taiwan University Hospital and National Taiwan University, Taipei, Taiwan; ¹⁴Department of Neurosurgery, China Medical University Hospital, Taichung, Taiwan; ¹⁵School of Medicine, ¹⁶Department of Surgery, China Medical University Hospital, and ¹⁷China Medical University Children's Hospital, China Medical University, Taichung, Taiwan; ¹⁸Department of Biotechnology, Asia University, Taichung, Taiwan

Edited by Patrick Sung

The pandemic caused by severe acute respiratory syndrome coronavirus 2 (SARS-CoV-2) has severely affected human lives around the world as well as the global economy. Therefore, effective treatments against COVID-19 are urgently needed. Here, we screened a library containing Food and Drug Administration (FDA)-approved compounds to identify drugs that could target the SARS-CoV-2 main protease (M^{Pro}), which is indispensable for viral protein maturation and regard as an important therapeutic target. We identified antimalarial drug tafenoquine (TFQ), which is approved for radical cure of *Plasmodium vivax* and malaria prophylaxis, as a top candidate to inhibit M^{Pro} protease activity. The crystal structure of SARS-CoV-2 M^{Pro} in complex with TFQ revealed that TFQ non-covalently bound to and reshaped the substrate-binding pocket of M^{Pro} by altering the loop region (residues 139–144) near the catalytic Cys145, which could block the catalysis of its peptide substrates. We also found that TFQ inhibited human transmembrane protease serine 2 (TMPRSS2). Furthermore, one TFQ derivative, compound 7, showed a better therapeutic index than TFQ on TMPRSS2 and may therefore inhibit the infectibility of SARS-CoV-2, including that of several mutant variants. These results suggest new potential strategies to block infection of SARS-CoV-2 and rising variants.

The severe acute respiratory syndrome coronavirus 2 (SARS-CoV-2) was identified in December 2019 as the cause of COVID-19 outbreak (1–3). It has since spread rapidly,

infected more than 180 million people, and caused more than 3.9 million deaths (4, 5) globally in late June of 2021. While various kinds of vaccines have been available and large number of people have received, and preliminary analyses from the United States and other countries also showed that a COVID-19 vaccination series is effective against SARS-CoV-2 infection (6–8). However, only about 22% of the world population has received at least one dose of an approved vaccine in late June of 2021 (9). At the current global vaccination rate, it is estimated to take at least 4.6 years to achieve worldwide herd immunity (70–85% of the population having received a two-dose vaccine) against COVID-19. This long-time gap will allow variants of the virus to develop and spread, potentially rendering current vaccines ineffective (9, 10). Recently, several novel variants of SARS-CoV-2 with various mutations and deletions in the RBD of spike protein have appeared in multiple countries. In the middle of 2020, spike gene analysis of SARS-CoV-2 revealed that a mutation on D614G substitution became more common as the pandemic spread (11). Furthermore, The B.1.1.7 (Alpha) variant, which has D614G mutation and N501Y mutation in spike protein, was first identified in the United Kingdom in 2020 and spread rapidly (12). Subsequently, three more variants of concerns are documented including B.1.351 (Beta) variant in South Africa, P.1 (Gamma) variant in Brazil, and B.1.617, B.1.618, and B.1.617.2 (Delta) from India. Except for variants from India, the other two variants harbor N501Y mutation on RBD, which increases binding affinity to ACE2 (13). In addition, P.1 variant has an escape mutation E484K, which is able to escape the host's immune defenses by the neutralizing antibody (14, 15). The B.1.617 variant became one of the leading variants from

* These authors contributed equally to this work.

* For correspondence: Mien-Chie Hung, mhung@cmu.edu.tw; Yeh Chen, bluecrystalprotein@gmail.com.

Inhibition of SARS-CoV-2 virus infection by tafenoquine and its derivatives

India spread to about 40 nations since January 2021 (16). It carries two important mutations, E484Q and L452R. Residues 452 and 484 could play a role in resistance to antibody neutralization. Both are separately found in many other coronavirus variants, but they have been reported together for the first time in B.1.617 (17, 18). Another variant from India, B.1.618, has a specific mutation Δ 145 to 146 (19). Residues 145 and 146 are known as antibody-binding sites (20). The B.1.617.2 is a variant of lineage B.1.617 and has most recently become a variant of concern and named as Delta variant on 31 May 2021 by the World Health Organization. Accordingly, Pfizer utilized vaccine (BNT162b2)-induced human sera to neutralize SARS-CoV-2 lineage B.1.1.7 pseudovirus, with slightly reduced activity compared with the original strain (21). However, the Moderna mRNA-1273 vaccine showed a five- to tenfold reduction in efficacy against the B.1.351 strain bearing the E484K mutation compared with pseudovirus bearing the D614G mutation (22). Therefore, any improvement of vaccine and anti-SARS-CoV-2 drugs is urgently needed in order to combat the COVID-19 pandemic. Currently, several clinical trials have demonstrated that remdesivir (23, 24) and dexamethasone (25) improve the prognosis in patients with SARS-CoV-2 infection. Until now, remdesivir and dexamethasone have been used for patients who are hospitalized with moderate and severe COVID-19 symptoms in most countries (26). Monoclonal antibodies (bamlanivimab and etesevimab) are another option of therapeutic agents only for the nonhospitalized patients with mild-to-moderate COVID-19 symptoms (27). However, the efficacy of remdesivir is limited (23, 28, 29) and dexamethasone is an anti-inflammatory drug, which does not directly inhibit virus replication. Hence, we need to continue to rapidly develop effective drugs, especially using the screening strategies for anti-SARS-CoV-2 therapeutics. The Food and Drug Administration (FDA)-approved drugs have undergone rigorous evaluations for safety, and it would be an advantage to screen compound library containing FDA-approved drugs as they can be quickly applied for treating patients.

The SARS-CoV-2 genome shares about 82% identity with the SARS coronavirus and contains approximately 30,000 nucleotides that are transcribed into 13 to 15 open reading frames (Orfs) (30). Among them, Orf1a and Orf1ab are translated into two polypeptides, which are then cleaved by the M^{pro} , yielding a number of protein products required for viral replication and transcription (31–34). Another critical cell surface protease for mediating virus entry into host cells is TMPRSS2, which trigger cell membrane fusion and uptake of SARS-CoV-2 (35). Because M^{pro} and TMPRSS2, which digest their substrates at each specific polypeptide sequences, are necessary for viral replication and infection respectively, these two proteases are considered as ideal targets for drug design. To this end, we firstly identified antiviral compounds from a library containing FDA-approved drugs, which can bind to M^{pro} and inhibit its enzymatic activity through a well-established fluorescence resonance energy transfer (FRET)-based high-throughput drug screening platform. Here, we found that an US FDA-approved drug tafenoquine (TFQ) not

only represses M^{pro} protease activity through inducing its conformational change, but also targets the cellular protease TMPRSS2 to display a dual function against SARS-CoV-2 activity. In addition, through medicine chemistry approaches, we synthesized 14 derivatives of TFQ and based on therapeutic index, therapeutic efficacy/toxicity, we identified one compound, compound 7 as a safer therapeutic agent than parental TFQ. Importantly, both TFQ and compound 7 suppressed viral infection including several variants through viral pseudoparticle (Vpp) assay.

Results

TFQ is a potential inhibitor of SARS-CoV-2 M^{pro}

To rapidly identify potential FDA-approved drugs targeting SARS-CoV-2 M^{pro} , we utilized an established FRET assay to screen 1836 compounds from FDA-Approved Drug Library (MedChemExpress, Cat. No.: HY-L022P) (36). Among the identified positive candidates, TFQ exhibited the most significant inhibitory effect against SARS-CoV-2 M^{pro} (Fig. 1A and Table S1). The half-maximal inhibitory concentration (IC_{50}) of TFQ against SARS-CoV-2 M^{pro} is 31.8 μ M (Fig. 1B). TFQ (brand name Krintafel/Kozenis in the United States/Australia, owned and developed by GlaxoSmithKline) is an 8-aminoquinoline antimalarial drug that was approved by the US FDA in July 2018 and the Australian Therapeutic Goods Administration (TGA) in September 2018 for the radical cure of *Plasmodium vivax* (37–39), a parasite that causes malaria. In addition, TFQ (brand name Arakoda/Kodatef in the United States/Australia, owned by 60 Degrees Pharmaceuticals) was later approved by the FDA and the TGA for malaria prophylaxis (39, 40). However, the molecular target of TFQ is still unknown. Here, we showed that TFQ directly inhibited SARS-CoV-2 M^{pro} *in vitro*. Another quinoline-based drug, Hydroxychloroquine (HCQ), a 4-aminoquinoline derivative, has shown to be effective in inhibiting SARS-CoV-2 infection *in vitro* (41). However, using HCQ for prevention or treatment of severe COVID-19 patients has shown no benefits or has severe side effects (42–44). To further characterize TFQ, we compared the inhibitory effects of TFQ and HCQ by using differential scanning fluorimetry (DSF), which is a powerful tool in early drug discovery with the basic principle that drugs that bind to the therapeutic protein target will change its thermal stability (45, 46). The result showed that TFQ caused thermal shifts in the melting temperature (T_m) of SARS-CoV-2 M^{pro} in a dose-dependent manner (Fig. 1C). In contrast, HCQ had no influence on the thermal stability of SARS-CoV-2 M^{pro} (Fig. 1D), supporting that TFQ may bind to M^{pro} and serve as a candidate to inhibit SARS-CoV-2 M^{pro} .

TFQ binding reduced the helical content of SARS-CoV-2 M^{pro}

To further validate the binding and inhibitory effects of TFQ on SARS-CoV-2 M^{pro} , various biophysical methods were utilized to assess the conformational changes of SARS-CoV-2 M^{pro} . Analytical ultracentrifugation (AUC) studies revealed identical sedimentation coefficient at various concentrations of TFQ, suggesting that the overall quaternary structure of

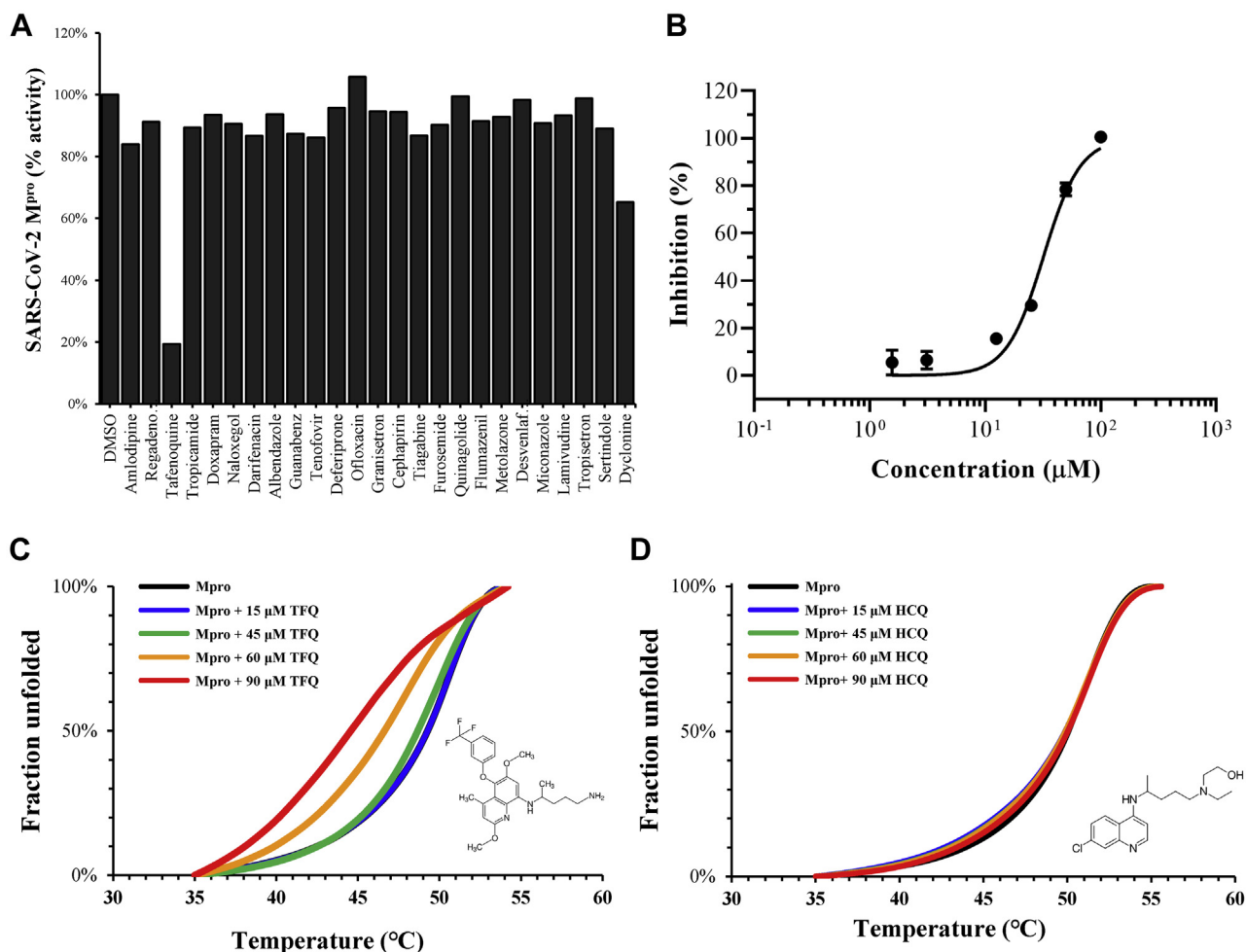


Figure 1. TFQ efficiently inhibits SARS-CoV-2 M^{pro}. **A**, screening of a library of FDA-approved compounds against SARS-CoV-2 M^{pro} by FRET assay. Each compound (60 μM) was pre-incubated with 4 μM of SARS-CoV-2 M^{pro} for 30 min at room temperature. Fluorescent protein substrate (20 μM) was then added to initiate the reaction. The relative enzymatic activity of SARS-CoV-2 M^{pro} is shown. **B**, dose–response curve of TFQ against SARS-CoV-2 M^{pro} with an IC₅₀ value of 31.8 μM. Data are shown as mean ± standard deviation, n = 3 technical replicates. **C**, melting curves of SARS-CoV-2 M^{pro} at various concentrations of TFQ (0, 15, 45, 60, 90 μM). **D**, melting curves of SARS-CoV-2 M^{pro} at various concentration of HCQ (0, 15, 45, 60, 90 μM). FRET, fluorescence resonance energy transfer; SARS-CoV-2, severe acute respiratory syndrome coronavirus 2; TFQ, tafenoquine.

SARS-CoV-2 M^{pro} remains unchanged in the presence of TFQ (Fig. 2A). Results from circular dichroism (CD) spectroscopy exhibited an increase in the far-UV signals (molar ellipticity at 222 nm) with increasing concentrations of TFQ, indicating that the total helical content of SARS-CoV-2 M^{pro} decreased upon TFQ binding (Figs. 2B and S1). In addition, the relative activity of SARS-CoV-2 M^{pro} decreased with increasing concentrations of TFQ (Fig. 2B), supporting the notion that total helical content of SARS-CoV-2 M^{pro} correlates with relative SARS-CoV-2 M^{pro} activity. To further evaluate the conformational changes of SARS-CoV-2 M^{pro}, we performed a limited proteolysis assay by trypsin digestion (47). The cleavage pattern, unexpectedly, indicated a greater degree of protection of SARS-CoV-2 M^{pro} from trypsin digestion at higher concentrations of TFQ, which was independent of any effect of TFQ on trypsin activity (Figs. 2C and S2). In contrast, HCQ did not reduce the cleavage of SARS-CoV-2 M^{pro} by trypsin digestion (Fig. 2C). These findings suggest that TFQ binding not only reduces the helical content but also induces local

conformational changes in SARS-CoV-2 M^{pro}, resulting in resistance to trypsin digestion.

Structural characterization of SARS-CoV-2 M^{pro} in complex with TFQ

To investigate the inhibitory effect of TFQ on SARS-CoV-2 M^{pro}, we established a cocrystallization structure of TFQ-M^{pro} complex (Table S2). The structure revealed that TFQ non-covalently binds to the active site of SARS-CoV-2 M^{pro} with a unique binding pattern that is distinctly different from the known covalent peptidomimetic inhibitors (Figs. 3A and S3A) (48). The hydrophobic quinoline core of TFQ locates near the catalytic dyads of SARS-CoV-2 M^{pro} and forms a hydrogen bond with the side chain of H41 on SARS-CoV-2 M^{pro}, blocking the access of substrates into the active site (Fig. 3A). The pentan-1,4-diamine moiety of TFQ buries deeply into the S2 subsite, interacting with residues T25, L27, C44, T45, S46, M49, and Q189 of SARS-CoV-2 M^{pro} with the terminal amino

Inhibition of SARS-CoV-2 virus infection by tafenoquine and its derivatives

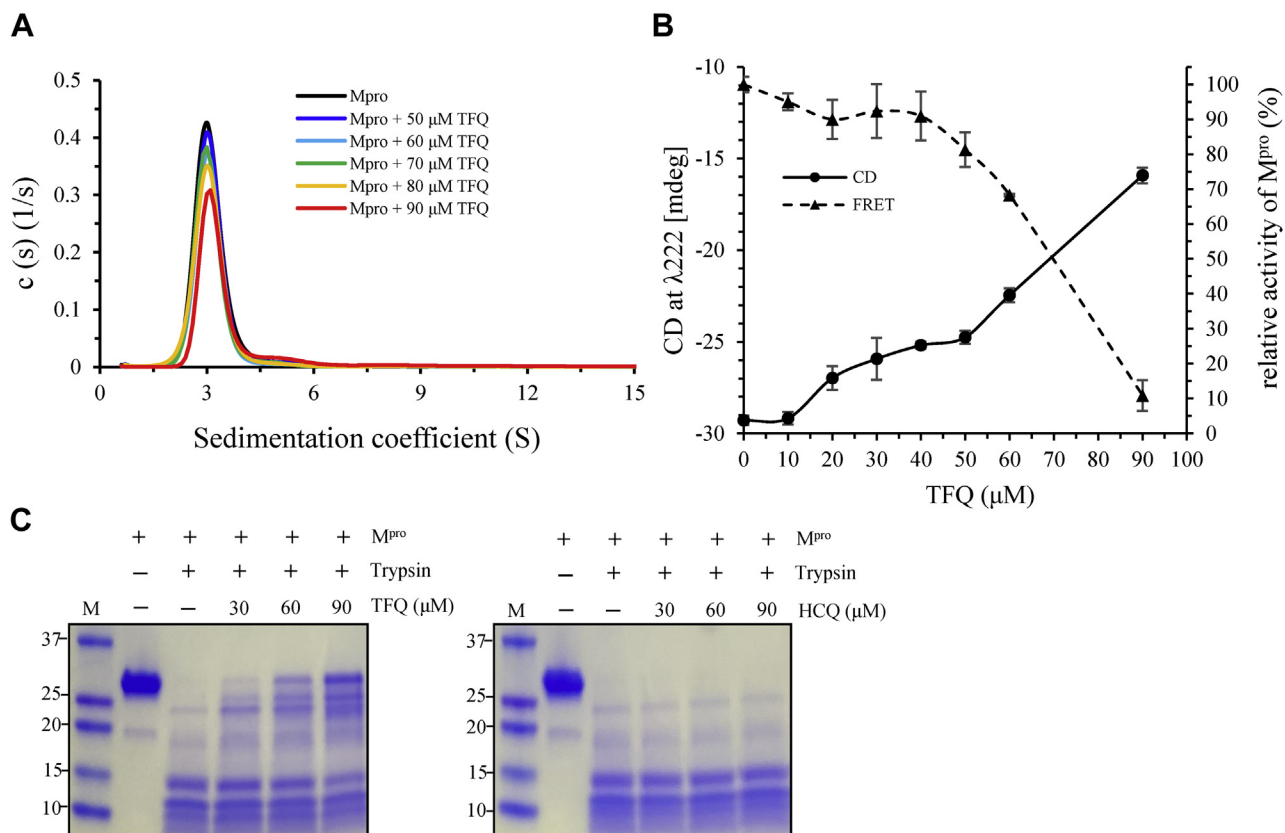


Figure 2. Inhibition of enzymatic activity of SARS-CoV-2 M^{pro} by TFQ. *A*, analytical ultracentrifugation (AUC) experiment of SARS-CoV-2 M^{pro} in the presence of different concentrations of TFQ (0, 50, 60, 70, 80, 90 μM). *B*, comparison of the enzymatic activity of SARS-CoV-2 M^{pro} with the far-UV CD signals (molar ellipticity at 222 nm) by increasing dose of TFQ. The results are shown as a *solid line* (CD signals) or *dashed line* (enzyme activity measured by FRET) with error bars from at least two replicates. *C*, limited proteolysis of SARS-CoV-2 M^{pro} by trypsin in the presence of different concentrations of TFQ (*left*) or HCQ (*right*) (0, 30, 60, 90 μM). CD, circular dichroism; FRET, fluorescence resonance energy transfer; SARS-CoV-2, severe acute respiratory syndrome coronavirus 2; TFQ, tafenoquine.

group of pentan-1,4-diamine moiety forming two hydrogen bonds with the main-chain oxygen of H41 and C44 of SARS-CoV-2 M^{pro} (Figs. 3, A and B and S3A). The trifluoromethylphenoxy moiety of TFQ forms hydrophobic interactions with L141, N142, and G143 in the S1 subsite of SARS-CoV-2 M^{pro}, which is further stabilized by two H-bonds between the two fluoride atoms and the main chain of G143 (Fig. 3, A and B). This interaction induces significant conformational changes in the loop region containing residues 139 to 144 in SARS-CoV-2 M^{pro}, which may otherwise cause steric clashes with the trifluoromethylphenoxy moiety of TFQ in the ligand-free form of SARS-CoV-2 M^{pro} (Fig. 3, C and D). The rotation of residues N142, L141, and F140 leads to the flipping of hydrophobic side chain of F140 into solvent and L141 into the S1 subsite (Fig. 3, A and D). Binding of TFQ also widens the substrate-binding pocket by 18.6 Å (measured by the distance between side chain of Q189 and N142) in contrast with the ligand-free form (10.9 Å) and the peptide-based inhibitor bound form (9.6 Å) of SARS-CoV-2 M^{pro} (Fig. S3, B–D). In summary, the abovementioned functional and structural data support local conformational changes in the substrate-binding pocket of SARS-CoV-2 M^{pro} and may provide relevant information to conduct structural modifications of TFQ.

In addition to the therapeutic importance of SARS-CoV-2 M^{pro}, TMPRSS2 is a host protease on cell membrane to

facilitate SARS-CoV-2 entry into host cells. The recent study indicated that the rapid transmissibility of B.1.617 variant from India could be attributed to its increased ability to enter human intestinal and lung cell lines and that specific TMPRSS2 inhibitor is effective against B.1.617 variant (49). Interestingly, we also observed TFQ to inhibit TMPRSS2 protease activity in a dose-dependent manner (Fig. S4), suggesting that TFQ could block SARS-CoV-2 by inhibiting enzymatic activities of both SARS-CoV-2 M^{pro} and host TMPRSS2.

TFQ inhibits SARS-CoV-2 production in cell culture system

Next, we examined the antiviral efficacy of TFQ on the viral production and infection rates of SARS-CoV-2. Vero E6 cells, which are kidney epithelial cells isolated from an African green monkey and commonly used to produce SARS-CoV-2 (36, 50) were infected with SARS-CoV-2 (strain NTU02, GenBank:MT066176.1) at a multiplicity of infection (MOI) of 0.001 in the presence of TFQ (2.5 μM and 5 μM) or DMSO (control). Cells were subjected to either pretreated plus posttreated with TFQ before and after viral infection (full-time treatment) or only treated with TFQ after virus infection (posttreatment) (Fig. 4A). After infection, cell supernatants were collected for further quantification of virus counts on day 1, day 2, and day 3, respectively. The inhibition rate of

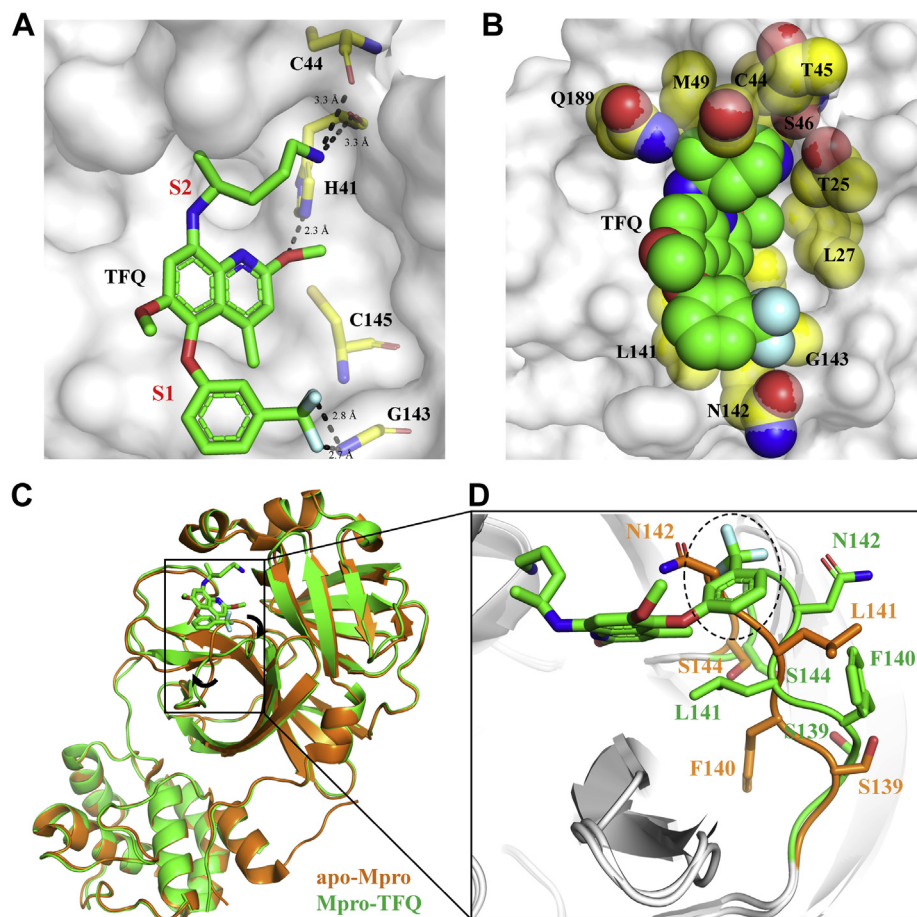


Figure 3. Structural analysis of TFQ interaction with SARS-CoV-2 M^{pro}. A, surface presentation of potential substrate-binding pocket of SARS-CoV-2 M^{pro} with TFQ. TFQ (green stick) interact with SARS-CoV-2 M^{pro} by forming hydrogen bonds (black dash line) on several residues (yellow stick) on SARS-CoV-2 M^{pro}. The S2 and S1 subsites of SARS-CoV-2 M^{pro} are indicated. B, detailed hydrophobic interactions between TFQ (green) and the active-site residues of SARS-CoV-2 M^{pro} (yellow). C, structural comparison of ligand-free form (orange) and TFQ bound form (green) of SARS-CoV-2 M^{pro}. The largest structural changes induced by TFQ binding occurring at the loop region containing residues 139 to 144 and indicated by black arrows. D, the detailed view of the altered loop region (residues 139–144) in (C). The potential steric clash between TFQ and the residue N142 from ligand-free form of SARS-CoV-2 M^{pro} is highlighted by a dashed black circle. SARS-CoV-2, severe acute respiratory syndrome coronavirus 2; TFQ, tafenoquine

TFQ against SARS-CoV-2 was determined by quantitative real-time RT-PCR (qRT-PCR) measuring viral RNA of nucleoprotein (N). The results indicated that TFQ significantly repressed the yield of viral RNA in cell supernatant on day 1 to 2 after infection (Fig. 4B). The inhibition rate against viral RNA production was approximately 0 to 3.5 % and 51.9 to 54 % with 5 μ M and 2.5 μ M TFQ, respectively, at 48-h post infection, implying that the half maximal effective concentration (EC₅₀) of TFQ was around 2.5 μ M (Fig. 4C). Viral infection can lead to changes in cell morphology and death of host cells, also known as cytopathic effect (CPE) (51, 52). Vero E6 cells are susceptible to SARS-CoV-2 infection, which induces CPE (53). We observed a significant decrease in SARS-CoV-2-induced CPE in Vero E6 cells treated with 5 μ M TFQ treatment compared with the DMSO treatment group (Fig. 4D), indicating that TFQ mitigates cell damages caused by SARS-CoV-2. Therefore, the data in Figure 4B observed on day 3 showed that there is no significant difference of viral RNA between DMSO-treated and TFQ (2.5 μ M)-treated groups because the former lacked sufficient number of surviving host cells for virus production. Collectively, these data

demonstrated that TFQ reduced SARS-CoV-2 production in the host cells.

Cell-based immunofluorescence assay revealed inhibition of SARS-CoV-2 M^{pro} in HEK-293T cells by TFQ treatment

To further investigate whether the inhibition effect of TFQ on SARS-CoV-2 production is mediated through M^{pro}, we established two stable HEK-293T cell lines expressing M^{pro}-CFP-YFP or M^{pro}-GFP-RFP fusion proteins. The M^{pro} cleavage site is placed between the CFP-YFP and GFP-RFP fusion proteins to evaluate the SARS-CoV-2 M^{pro} activity using fluorescence detection. SARS-CoV-2 M^{pro} fusion protein is accommodated with CFP-YFP or GFP-RFP by the F2A enhancing fusion. The results showed that SARS-CoV-2 M^{pro} has an activity that cleaved GFP and RFP at the cleavage site and separated GFP-RFP with the single fluorescent expression in the cell under microscopy determination (Fig. S5). The endogenous fluorescence is reversed and combined significantly with the M^{pro} activity inhibition by TFQ treatment (50 and 100 μ M) in the HEK-293T cells (Fig. S5). The inhibition of

Inhibition of SARS-CoV-2 virus infection by tafenoquine and its derivatives

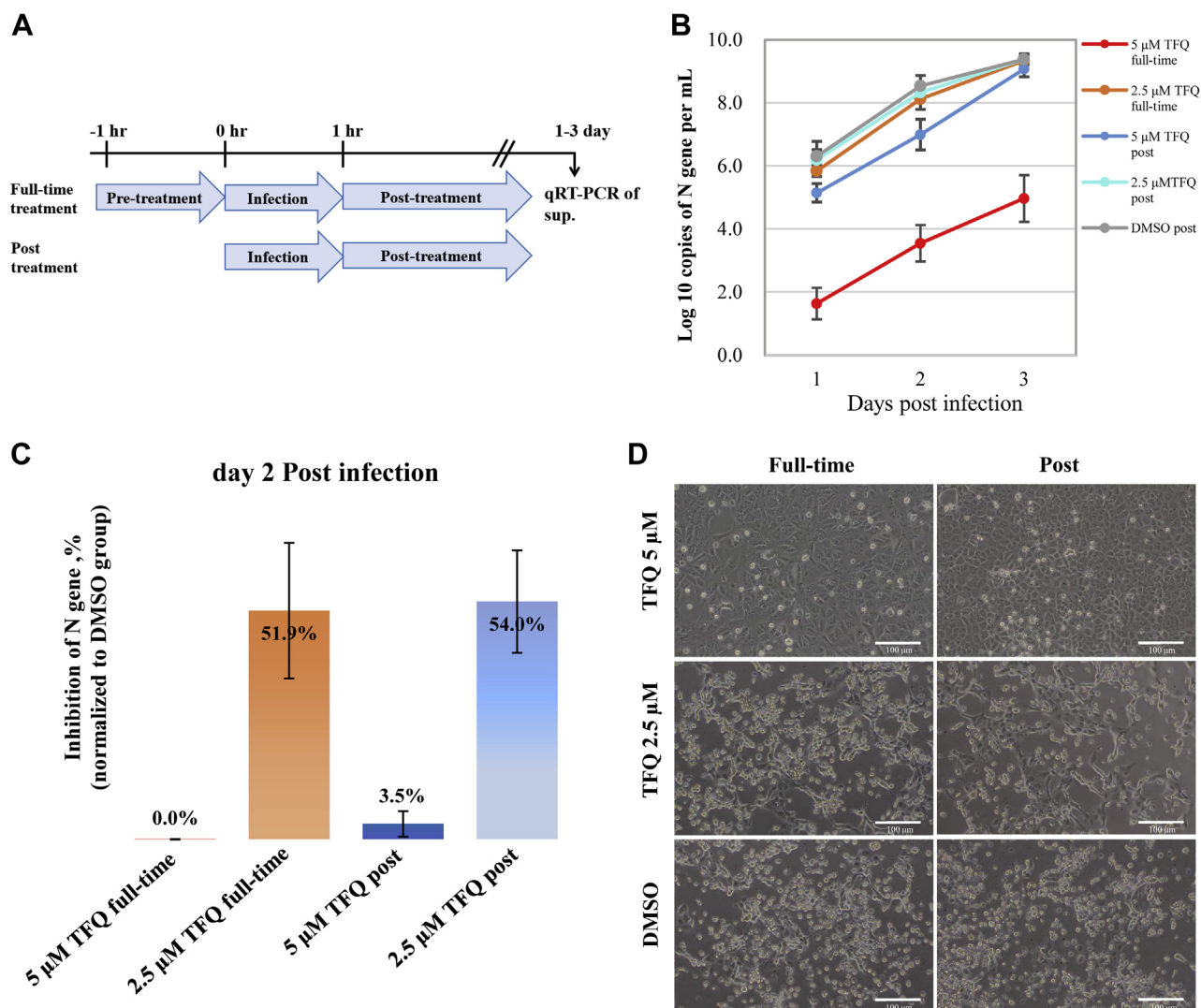


Figure 4. TFQ represses SARS-CoV-2 infection in Vero E6 cells. A, a schematic illustrating two methods of treatments of TFQ in SARS-CoV-2 infected Vero E6 cells. In the posttreatment group, cells were treated with TFQ after viral infection. In the full-time treatment group, cells were pretreated with TFQ for 1 h prior to viral infection plus the posttreatment of TFQ after viral infection. B, the virus-infected Vero E6 cells were treated with TFQ (2.5 and 5 μM) or DMSO. The cell supernatant was collected on day 1, day 2, and day 3 and then subjected to qRT-PCR to determine the viral titer ($n = 3$). Data are shown as mean \pm standard deviation. C, the inhibition rate of virus infection on day 2 in Vero E6 cells treated with 2.5 or 5 μM TFQ with full-time or posttreatment ($n = 3$). Data are shown as mean \pm standard deviation. D, 10 \times phase-contrast images of virus-infected Vero E6 treated with DMSO or TFQ (2.5 μM and 5 μM) with TFQ full-time or posttreatment at 3 days post infection. SARS-CoV-2, severe acute respiratory syndrome coronavirus 2; TFQ, tafenoquine.

M^{pro} activity by TFQ was also confirmed by FRET detection in the HEK-293T cell lysates (Fig. S6). In the presence of SARS-CoV-2 M^{pro} activity, FRET detection was reduced. Addition of 100 μM TFQ consistently lowered SARS-CoV-2 M^{pro} activity, resulting in a twofold increase in FRET percentage (Fig. S6). Taken together, these *in vivo* data suggested that despite being at high dose, TFQ inhibited SARS-CoV-2 production through M^{pro} , which is also consistent with the result of *in vitro* M^{pro} activity analysis (Fig. 1B).

Pharmacological exploitation of TFQ to develop a novel, noncytotoxic TMPRSS2 inhibitor

TFQ blocked SARS-CoV-2 viral infection (Fig. 4), at least in part, by inhibiting the enzymatic activity of viral M^{pro} (Fig. 1)

and host TMPRSS2 proteases (Fig. S4). As shown in Fig. S7, C and D, TFQ was equipotent in inhibiting both enzyme activities. TFQ exhibits CPE at 5 μM (Fig. 4), thus the therapeutic window may be limited to develop into a clinically useful drug. We turned our attention to the use of TFQ as a base compound to develop specific, noncytotoxic inhibitors as therapeutic intervention for COVID-19 (54, 55). Based on the structural information shown in Figure 3, we employed two different strategies to conduct structural modifications of TFQ to develop M^{pro} and TMPRSS2 inhibitors, which is delineated as follows. Our initial effort focused on the direct derivatization of TFQ by substituting or replacing the aniline amino moiety and/or the terminal-NH₂ of the alkyl side chain with different functionalities, leading to compounds 1 to 6 (Fig. S7B). However, these compounds with the exception of compound 3

showed substantially reduced inhibitory activities toward both proteases (Fig. S7, B–D). In compound 3, the N-monomethylation at the terminal-NH₂ retained the TMPRSS2 inhibitory activity, but gave rise to a partial loss of the M^{Pro} inhibitory activity, which might be attributable to steric hindrance imposed by the N-CH₃ substitution for ligand interactions with the H41 and C44 residues of M^{Pro} (Fig. 3). This premise was corroborated by losses of the M^{Pro} inhibitor activity to a greater extent in compounds 2 and 4 by adding an additional N-methyl function to either the terminal-NH₂ or the aniline-NH, respectively (Fig. S7C). Interestingly, compounds 2 and 4 also showed a complete or significant loss of the TMPRSS2 inhibitory activity (Fig. S7D), suggesting the importance of the terminal-NH₂ in the mode of ligand binding with TMPRSS2. It is interesting that an additional N-methyl function at either the terminal-NH₂ (compound 2) or the aniline-NH (compound 4) resulted in a complete loss of the TMPRSS2 inhibitory activity (Fig. S7, B–D). Replacement of the terminal-NH₂ moiety of TFQ with a guanidino (compound 5) or thiourea (compound 6) group, which was aimed at enhancing potential hydrogen bonding with the H41 and C44 residues of M^{Pro} (Fig. 3), led to a complete loss of both inhibitory activities presumably due to steric hindrance (Fig. S7, B–D). Together, these data suggest a subtle structure–activity relationship, which prompted us to take an alternative fragment-based strategy by selecting compound 7, a key intermediate in TFQ synthesis, as a starting point for modifications (Fig. S8A). We coupled compound 7 with terminal NH₂-containing alkyl or acyl side chains with varying lengths (Series I, compounds 8–10) or with different amino acids [Series II, including L-asparagine, L-glutamine, L-lysine, and L-ornithine, compounds 11–14, respectively] (Fig. S8A). We rationalized that these changes might allow a better differentiation of the binding pocket of TMPRSS2 *versus* M^{Pro} by these small-molecule compounds. It is noteworthy that among these eight derivatives (7–14), compound 7 exhibited a nearly effective TMPRSS2 inhibitory activity relative to TFQ, while deficient in M^{Pro} inhibition (Fig. S8, B and C). Moreover, compounds 8 and 13 also showed discriminative inhibitory activities between TMPRSS2 and M^{Pro} in favor of the former (Fig. S8, B and C). This loss of M^{Pro} inhibitory activity in compounds 8 and 13 underlies the stringent requirement of the length of the aminoalkyl side chain in directing the interaction of the terminal-NH₂ with the H41 and C44 residues of M^{Pro}, as depicted in Figure 3.

The compound 7 is a potential drug candidate for COVID-19

Since a crucial issue of TFQ is its narrow safety margin for clinical treatment, it is important to determine the cytotoxicity of these TFQ-derived compounds. After the cytotoxicity screening by using MTT assay in the Vero E6 and Calu3 cells, we found that one of the TFQ-derived compounds, compound 7, had the highest drug safety in both cell lines (Fig. 5, A and B). To further measure the CC₅₀ (50% cytotoxic concentration) of compound 7 compared with TFQ, the results showed that

compound 7 had an CC₅₀ value tenfold higher than TFQ in both Vero E6 and Calu3 cell lines (Fig. 5, C and D). As the aminoalkyl side chain of TFQ was truncated in compound 7, these results suggested the role of this substructure in contributing not only to the M^{Pro} inhibitory activity but also to cytotoxicity of TFQ (Fig. 5E).

To further examine the potential activity of compound 7 in SARS-CoV-2 infection, SARS-CoV-2 pseudovirus assay was employed in human bronchial epithelial Calu-3 and monkey kidney epithelial Vero E6 cells, respectively. Recent reports indicated that there are two major entry pathways of SARS-CoV-2, either through the ACE2-endosomal pathway or *via* TMPRSS2 at the cell surface (56). Vero E6 cells, a common cell line for the SARS-CoV-2 study, have high ACE2 expression levels but with low TMPRSS2 expression. This finding suggests a link between SARS-CoV-2 entry and the ACE2-endosomal pathway in Vero E6 cells. On the other hand, as Calu3 cells express a high level of TMPRSS2, SARS-CoV-2 entry into Calu3 cells might be TMPRSS2-dependent. In light of the high potency of compound 7 in TMPRSS2 inhibition, we further established a TMPRSS2-expressing system in both cell lines (Fig. 6A). These cells were pretreated with HCQ, TFQ, or compound 7 for 1 h and then infected with the SARS-CoV-2 Vpp. After 24 h of incubation, infection efficiency was measured according to luciferase activities. As HCQ is an inhibitor of the endosomal pathway, published reports showed that it does not block SARS-CoV-2 infection in the TMPRSS2-expressing cells (57). Indeed, results from three independent experiments showed that HCQ only blocked infection of SARS-CoV-2 Vpp in wild-type Vero E6 cells, but not in TMPRSS2-overexpressing cells (Fig. 6B). In contrast, both TFQ and compound 7 at high doses were more effective in inhibiting viral infection in TMPRSS2-overexpressing cells than that in the parental cells (Fig. 6, B and C). These results suggested that TFQ and compound 7 could inhibit SARS-CoV-2 Vpps likely through inhibiting TMPRSS2 activity. Indeed, the cell-based TMPRSS2 enzymatic assay revealed that both TFQ and compound 7 blocked protease activity of TMPRSS2 through competitive inhibition mode, and the inhibition constant K_i of them was determined to be 10.18 and 16.79 μ M, respectively (Fig. S9). Furthermore, compound 7 showed a much higher selectivity index (SI) than TFQ (Fig. 6D). Our finding suggested that the compound 7 may be a promising drug for blocking SARS-CoV-2-driven entry into host cells. Since there are more SARS-CoV-2 variants emerging, it is imperative to evaluate the inhibitory efficacy of TFQ and compound 7 against the entry of different SARS-CoV-2 variants. The VeroE6-TMPRSS2 cells were pretreated for 1 h with different concentrations of TFQ or compound 7 and then infected with five kinds of SARS-CoV-2 Vpp, including the wild-type, B.1.1.7, B.1.351, B.1.617, or B.1.618 variants, respectively. After 24 h of incubation, infection efficiency was measured by luciferase assay (Fig. 6, E and F). The results indicated that both the EC₅₀ and SI of TFQ or compound 7 were similar between wild type and each variant (Fig. 6, G and H). In conclusion, we found that compound 7

Inhibition of SARS-CoV-2 virus infection by tafenoquine and its derivatives

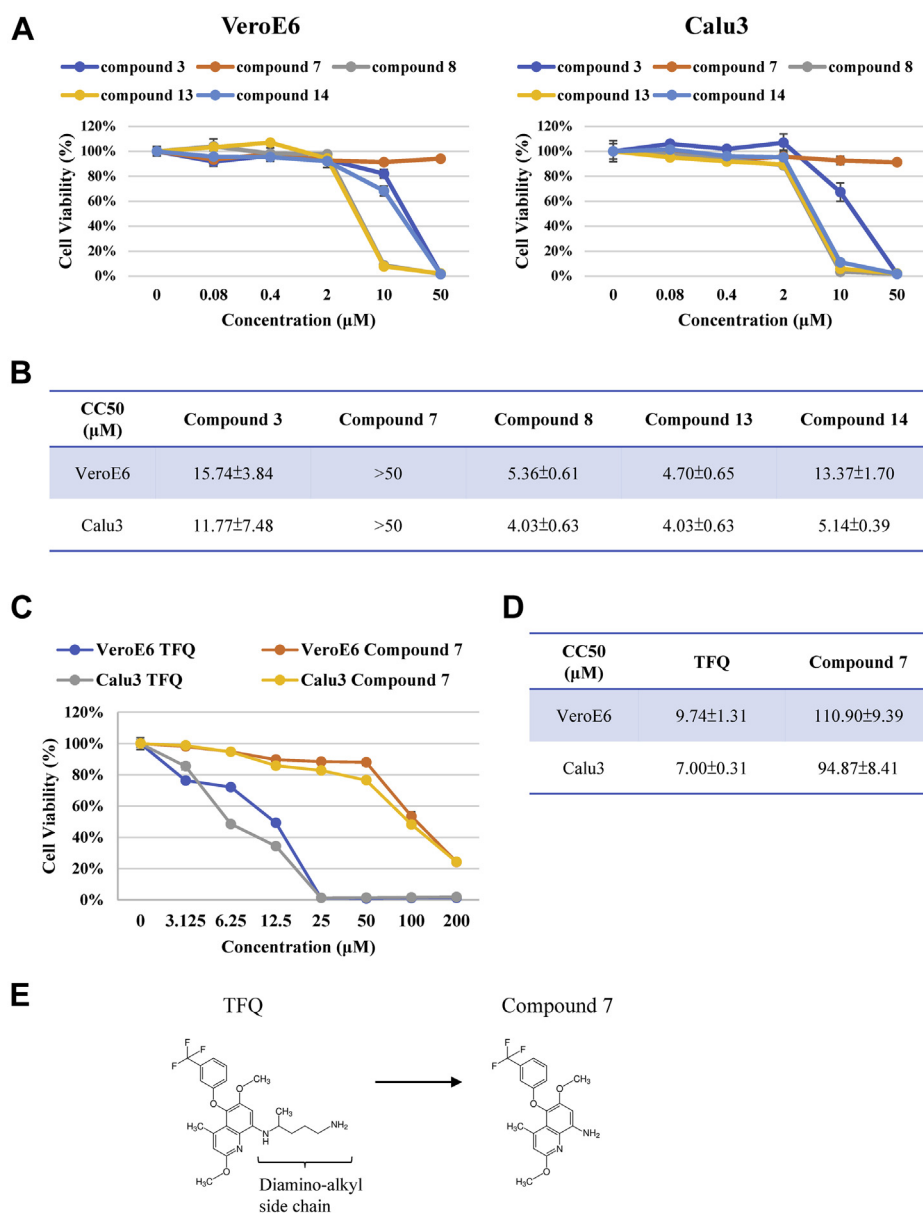


Figure 5. TFQ derivative Compound 7 exhibits a lower toxicity than that of TFQ. *A*, MTT assay of VeroE6 cells (*left panel*) and Calu3 cells (*right panel*) treated for 24 h with indicated concentrations of compound 3, 7, 8, 13, and 14. Each data point represents the average of values obtained in three independent experiments. Error bars represent the standard deviation of the means. *B*, the CC50 values of compounds 3, 7, 8, 13, and 14 were determined by using GraphPad PRISM software and expressed as mean \pm SD. *C*, VeroE6 and Calu3 cells were treated with varying concentrations of TFQ or compound 7, and cell viability was assessed by MTT assay. Error bars represent the standard deviation of the means. *D*, the CC50 values of TFQ and compound 7 were determined by using GraphPad PRISM software and expressed as mean \pm SD. *E*, the chemical structure of TFQ and compound 7 was presented. TFQ, tafenoquine.

could not only repress infectivity of wild-type SARS-CoV-2, but also different variants of mutant Vpp.

Discussion

Drug repurposing is an efficient way to accelerate the development of therapies for COVID-19. Here, we identified TFQ as a potential drug candidate that inhibits SARS-CoV-2 infection and replication by targeting its M^{PRO} and human TMPRSS2 from an FDA-approved compound library. We first demonstrated that TFQ inhibits both the enzymatic activity of SARS-CoV-2 M^{PRO} and human TMPRSS2 by using a

FRET-based assay. Subsequent functional studies including DSF, AUC, CD, and limited proteolysis assay indicated that SARS-CoV-2 M^{PRO} underwent local structural changes upon binding of TFQ under physiological relevant concentration. This conformational change induced by TFQ is positively correlated with the loss of enzyme activity of SARS-CoV-2 M^{PRO}. Structural characterization of TFQ-M^{PRO} complex further revealed that TFQ probably interferes with the substrate-binding site and catalytic subunit by reshaping of the active site and inducing significant conformational change of the loop region near catalytic residue Cys145. Indeed, the structural variations of the loop region near Cys145 have been

Inhibition of SARS-CoV-2 virus infection by tafenoquine and its derivatives

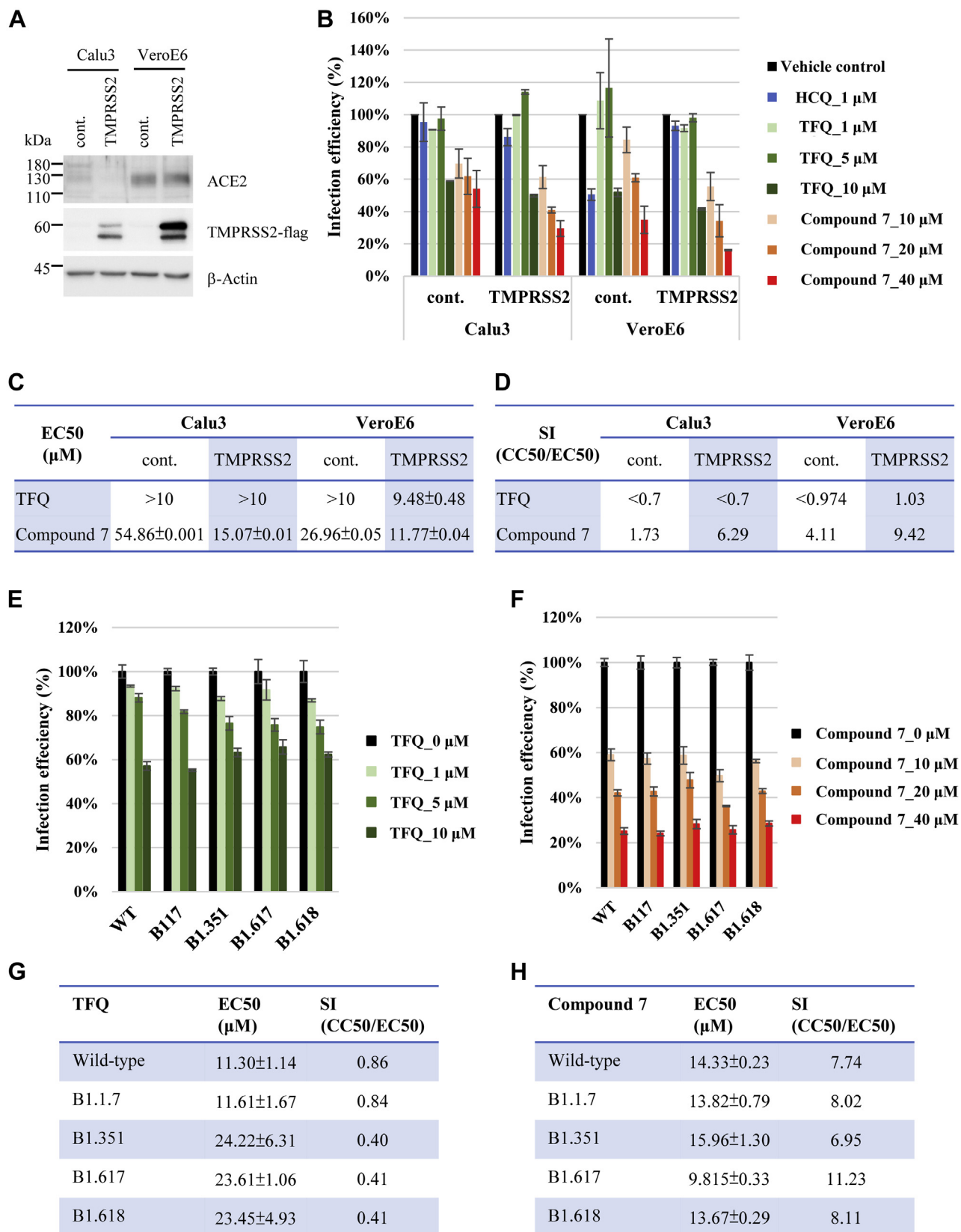


Figure 6. Compound 7 suppressed SARS-CoV-2 pseudovirus infection by TMPRSS2-dependent manner. A, immunoblot analysis of whole-cell lysates from vector control or TMPRSS2-expressing VeroE6 and Calu3 cells. B, Calu3 and VeroE6 cells with and without TMPRSS2 expression were pretreated with HCQ, TFQ or compound 7 and then infected with SARS-CoV-2 Spike pseudovirus. After 24 h of infection, the infection efficiency rate was measured by luciferase activities. Error bars represent the standard deviation of the means. C, the EC50 of TFQ and compound 7 was determined by GraphPad PRISM software, expressed as mean ± SD. D, the selectivity index (SI) of TFQ and compound 7 was measured by mean CC50/mean EC50. E and F, VeroE6 cells with TMPRSS2 expression were pretreated with indicated concentration of TFQ or compound 7 and then infected with SARS-CoV-2 Spike Wild-type, B1.1.7

Inhibition of SARS-CoV-2 virus infection by tafenoquine and its derivatives

previously observed in structure of SARS-CoV M^{Pro} in complex with benzotriazole esters or with acidic pH values (58, 59). Recently, a possibly catalytic incompetent conformation of SARS-CoV-2 M^{Pro} with large structural movements of N142 and F140 has also been reported (60). The structure of SARS-CoV-2 M^{Pro} complexed with Tafenoquine revealed in this study suggested that the structural plasticity of the substrate-binding pocket of M^{Pro} could be induced by ligand binding and thereby provide a new way for drug design.

Interestingly, several noncovalent, nonpeptidomimetic small-molecule compounds were also reported to inhibit SARS-CoV-2 M^{Pro} (61–63). For example, baicalein, ML188, and MUT056399 can bind to the active site and block access of the substrates to the catalytic dyad (61–63). In addition, pelitinib, ifenprodil, tofogliflozin, and AT7519 were discovered to bind to two newly identified allosteric sites of SARS-CoV-2 M^{Pro}, affecting its dimerization and thus the catalytic ability (62). In general, noncovalent inhibitors have the advantage of less off-target toxicity over covalent inhibitors (64). Moreover, covalent, peptidomimetic inhibitors are prone to proteolytic degradation, which limits their therapeutic application (65). For instance, the N3 inhibitor blocked SARS-CoV-2 at a concentration of 10 μ M in cell-based assay (48) whereas TFQ exhibited strong antiviral effect at a concentration of 5 μ M in SARS-CoV-2-infected Vero E6 cells (Fig. 4).

TFQ is approved for prophylaxis and treatment of malaria in the United States and Australia (40, 66). As a preventive measure, a dose of 200 mg TFQ is recommended for 3 days prior to traveling and 200 mg per week until 1 week after return. For radical cure, a single dose of 300 mg TFQ is recommended (<https://wwwnc.cdc.gov/travel/news-announcements/tafenoquine-malaria-prophylaxis-and-treatment>). Those above dose recommendations for malaria prophylaxis suggested that TFQ at higher doses may be suitable for human consumption. As shown in Figure 4, the therapeutic window of TFQ in cell culture may be limited, we thereby turn to develop potential drug candidate targeting both SARS-CoV-2 M^{Pro} and TMPRSS2 with higher safety using TFQ as scaffold. Although the TFQ-derived compound **1** to **14** did not exhibit significant inhibitory effect on SARS-CoV-2 M^{Pro}, it has provided useful structural and functional relationship. For example, the reduced inhibitory effects of compound **2** and **3** probably resulted from the monomethylation (compound **3**) and dimethylation (compound **2**) of the terminal-NH₂ group of the aminoalkyl side chain of TFQ that breaks the formation of hydrogen bonding to H41 and C44 according to our solved M^{Pro}-TFQ structure (Figs. 3A and S7C). Furthermore, the inverse relationship of the length of the aminoalkyl side chain of TFQ (Compound **7**–**10**, Fig. S8B) and their corresponding inhibitory effects suggested the importance of the hydrophobic interaction between this aminoalkyl side chain and the substrate-binding pocket of SARS-CoV-2 M^{Pro} as mentioned above (Fig. 3, A and B). Despite the absence of complex

structure of human TMPRSS2 with TFQ, we have identified TFQ-derived compound **7** as a novel, noncytotoxic inhibitor against TMPRSS2 in enzyme activity assay. The SARS-CoV-2 and its variants Vpp infection assay further showed that compound **7** has similar EC₅₀ values with TFQ in TMPRSS2-overproducing cell lines, but has a higher selectivity index than TFQ. The low cytotoxicity and potential inhibitory effect on TMPRSS2-dependent SARS-CoV-2 entry pathway of TFQ derived compound **7** should warrant further testing in clinical trials.

It is worth mentioning that SARS-CoV-2 variants have been outspread including those of variants from United Kingdom, South Africa, and India (67, 68) that have caused multiple waves of infections in several different countries. Thus, it is encouraging to identify TFQ and the derivative compound **7** that can inhibit infection activities of variants of mutant SARS-CoV-2.

Experimental procedures

Cells

TMPRSS2-expressing cells were generated by transient transfection with the pCMV3-TMPRSS2-Flag plasmid (Sino Biology) and selection by hygromycin. Calu3 and Calu3-expressing TMPRSS2 were cultured in Modified Eagle's Medium (MEM) supplemented with 10% fetal bovine serum (FBS), 1x NEAA, and 1% penicillin/streptomycin. Vero E6 and Vero E6-expressing TMPRSS2 were cultured in Dulbecco's Modified Eagle's Medium (DMEM) supplemented with 10% FBS, 1x GlutaMAX, and 1% penicillin/streptomycin. Both cell lines were incubated at 37 °C and 5% CO₂.

Cytotoxicity assay

The viability of cells after 24 h treatment was determined using the standard MTT [3-(4,5-dimethylthiazol-2-yl)-2,5-diphenyltetrazolium bromide] assay. All the treatments were done using 5 × 10³ cells/well in 96-well plate. The purple formazan crystals were dissolved in DMSO (100 μ l/well), and the absorbance was recorded on a microplate reader at a wavelength of 570 nm. The CC₅₀ values (50% cytotoxic concentration) were defined as the compound's concentration (μ M) required for the reduction of cell viability by 50% and were calculated by using GraphPad PRISM software.

Western blot assay

Cell lysates were collected by RIPA buffer plus protease inhibitors. The concentration of total protein was measured by Bradford protein assay. Protein was denatured at 95 °C for 5 min and loaded into SDS-PAGE to run. The SDS-PAGE was transferred to a PVDF membrane, and the membrane was blocked with 5% milk. After blocking, the membrane was immune-stained with indicated antibodies. All antibodies were diluted to a recognition level (1:1000) by using 5% BSA buffer

B.1.351, B.1.617, or B.1.618 pseudovirus. After 24 h of the infection, the infection efficiency rate was measured according to luciferase activities. Error bars represent the standard deviation of the means. G and H, the EC₅₀ (mean \pm SD) and SI value of TFQ and compound **7** were determined. SARS-CoV-2, severe acute respiratory syndrome coronavirus 2; TFQ, tafenoquine. TMPRSS2, TFQ inhibited human transmembrane protease serine 2.

Inhibition of SARS-CoV-2 virus infection by tafenoquine and its derivatives

and incubated at 4 °C overnight. After incubation with HRP-labeled secondary antibody, the chemoluminescence signal was catalyzed by ECL (Bio-Rad Laboratories) to detect the level of protein expression.

Virus and cell culture

SARS-CoV-2 (strain NTU02, GenBank:MT066176.1) was isolated from a COVID-19 patient at National Taiwan University Hospital and grown in Vero E6 cells. Cells were maintained in DMEM containing 10% FBS.

Viral infections

Vero E6 cells (1×10^7) were washed with PBS, incubated with virus diluted in serum-free DMEM containing tosylsulfonyl phenylalanyl chloromethyl ketone (TPCK)-trypsin (2 µg/ml) for 1 h at 37 °C at a MOI of 0.001. One hour after infection, the virus inoculum was removed. The infected cells were washed with PBS and incubated with fresh medium containing 2% FBS.

Viral pseudoparticles (Vpp) infection

In total, 5000 cells were seeded in 96-well plates. The next day, cells were preincubated with different compounds or DMSO (vehicle control) for 1 h. Then, they were infected with the Vpp harboring SARS-2-S and luciferase reporter purchased from National RNAi Core Facility (NRC), Academia Sinica, and followed by centrifugation at 1250g for 30 min. After 24 h incubation, the Cell Counting Kit-8 (CCK-8) assay (Dojindo Laboratories) was performed to measure the cell viability. Each sample was mixed with an equal volume of ready-to-use luciferase substrate Bright-Glo Luciferase Assay System (Promega) afterward. The relative light unit (RLU) was measured immediately by the GloMax Navigator System (Promega) and normalized with cell viability first, then the control group was set as 100%, and the relative infection efficiencies were calculated.

Recombinant protein preparation

The cloning, expression, and purification of SARS-CoV-2 M^{Pro} and its fluorescent protein substrate were described previously (36). Briefly, the *E. coli* BL21 (DE3) cells harboring the plasmid containing target gene were grown in Luria Broth medium at 37 °C until OD₆₀₀ reached 0.6 to 0.8. Overexpression of target protein was induced either by the addition of 0.2% L-rhamnose (for SARS-CoV-2 M^{Pro}) or 0.5 mM IPTG (for the fluorescent protein substrate) and incubated for 18 h at 20 °C. The cell pellets were resuspended in buffer containing 50 mM Tris-HCl pH 8.0, 500 mM NaCl, 10% glycerol, 1 mM TCEP, 1 mM PMSF, lysed by sonication, and centrifuged to remove cell debris and insoluble materials. The target protein was then purified by Ni-NTA chromatography using HisTrap FF column (GE Healthcare) according to the manufacturer's protocol. The fractions containing the expected size of SARS-CoV-2 M^{Pro} were pooled and mixed with adequate amount of TEV protease to remove the N-terminal SUMO fusion tag. Both TEV protease and His₆-SUMO fusion tag

were then removed by HisTrap FF column. For purity and monodispersity, the SARS-CoV-2 M^{Pro} and its substrate protein were further purified by gel filtration and stored in buffer containing 50 mM Tris-HCl pH 8.0, 200 mM NaCl, 5% glycerol, and 1 mM TCEP.

Small-molecule compound library

Three small-molecule compound libraries, including the FDA-approved Drug Library, Clinical Compound Library, and Anti-COVID-19 Compound Library (MedChemExpress), were used to screen for drugs against SARS-CoV-2 M^{Pro}.

Fluorescence resonance energy transfer (FRET) assay

SARS-CoV-2 M^{Pro} (4 µM) in assay buffer (20 mM Tris-HCl 7.8, 20 mM NaCl) was preincubated with or without 60 µM compounds for 30 min at room temperature in 96-well black Optiplate. The reaction was initiated by addition of 20 µM fluorescent protein substrate. Substrate cleavage was monitored continuously for 1 h by detecting the fluorescence signal (excitation: 434 nm/emission: 474 nm) using Synergy H1 hybrid multimode microplate reader (BioTek Instruments, Inc). The first 15 min of the reaction was used to calculate initial velocity (V_0) by linear regression. The calculated initial velocity with each compound was normalized to DMSO control. The IC₅₀ was calculated by plotting the initial velocity against various concentrations of TFQ by use of a dose-response curve in Prism 8 software.

For enzyme activity assay of human TMPRSS2, tested compounds were first incubated with TMPRSS2 protein at room temperature, and the fluorescent protein substrate was then added to start the reaction. The fluorescence signal was detected with excitation wavelength of 506 nm and emission wavelength of 536 nm.

Protein thermal shift assay using differential scanning fluorimetry

DSF assays were conducted as previously described (69). Briefly, the experiment was carried out on a CFX96 RT-PCR instrument (Bio-Rad) in a buffer comprising 25 mM Tris pH 8.0, 150 mM NaCl, 5X SYPRO Orange dye (Sigma-Aldrich), and 8 µM SARS-CoV-2 M^{Pro} in the presence or absence of various concentrations of TFQ or HCQ (15–90 µM) in each well. Fluorescence was monitored when temperature was gradually raised from 25 to 90 °C in 0.3 °C increments at 12-s intervals. Melt curve data were plotted using the Boltzmann model to obtain the temperature midpoint of unfolding of the protein using Prism 8.0 software (GraphPad).

Circular dichroism (CD) spectroscopy

CD signals were measured using a Jasco J-815 spectropolarimeter with 0.1-cm quartz cuvettes and a 1-mm slit width. The molar ellipticity at 222 nm of all samples was recorded to analyze the protein conformational changes at different concentrations of TFQ (0–90 µM). All spectra were corrected for buffer absorption.

Inhibition of SARS-CoV-2 virus infection by tafenoquine and its derivatives

Analytical ultracentrifugation (AUC)

To assess the quaternary structural changes of SARS-CoV-2 M^{Pro} in the presence of TFQ, sedimentation velocity experiments were performed using a Beckman Optima XL-A analytical ultracentrifuge (Beckman Coulter). Before ultracentrifugation, the protein sample was preincubated with or without various concentrations of TFQ (50–90 μ M) at room temperature for 30 min. The protein sample and buffer solutions (25 mM Tris 8.0, 150 mM NaCl) were separately loaded onto the double sector centerpiece and placed in a Beckman An-50 Ti rotor. The experiments were performed at 20 °C and at a rotor speed of 42,000 rpm. The protein samples were monitored by the UV absorbance at 280 nm in continuous mode with a time interval of 480 s and a step size of 0.002 cm. Multiple scans at different time points were fitted to a continuous size distribution model by the program SEDFIT (70). All size distributions were solved at a confidence level of $p = 0.95$, a best fitted average anhydrous frictional ratio (f/f_0), and a resolution N of 250 sedimentation coefficients between 0.1 and 20.0 S.

Limited proteolysis by trypsin

The protein sample was preincubated with or without various concentrations of TFQ or HCQ (30–90 μ M) at room temperature for 30 min. Proteolysis was then performed by mixing SARS-CoV-2 M^{Pro} (0.8 mg/ml) with trypsin (Sigma-Aldrich, T4799) at a protease-to-protein ratio of 1:10 (w/w) in reaction buffer (25 mM Tris 8.0, 150 mM NaCl) at 37 °C for 30 min. The reaction was stopped by adding SDS sample loading buffer and boiling at 95 °C for 10 min and subjected to SDS-PAGE (4–20%). To exclude the potential effect of TFQ on the protease activity of trypsin, a control experiment was performed using Trypsin Activity Assay Kit (Chondrex, Inc, Catalog # 3043). Briefly, 0.008 mg/ml trypsin was incubated with TFQ (0, 30, 60, 90 μ M) at the indicated concentration at room temperature for 30 min. Final concentration of 5 μ mole Boc-Gln-Ala-Arg-pNA substrate was then added to initiate the reaction. Releasing the p-nitroanilide (pNA) after substrate cleavage by trypsin was monitored by reading the optical density at 405 nm for 15 min. The trypsin activity after substrate cleavage for 15 min was calculated by the following equation: $(\text{OD}_{\text{Sample}} - \text{OD}_{\text{Blank}}) \times 5 \mu\text{mole}/(\text{OD}_{\text{Control}} - \text{OD}_{\text{Blank}}) \times 15 \text{ (minutes)} \times 0.1 \text{ (ml)}$.

In vivo detection of cleavage activity of SARS-CoV-2 M^{Pro} by immunofluorescence assay

To construct cell expression vectors, the *cfp-yfp* and *gfp-rfp* genes were amplified with following primers. The *cfp* forward primer 5'-CCAGGATCCATGG TTAGCAAGGGCGAG-GAAC-3' and *yfp* reverse primer 5'-AGACTCGAGTTTGTA-CAG TTCGTCCATACCCA-3'; *gfp* forward primer 5'-CCAGG ATCCGTTAGCAAGGGCGAGG AAGAC-3' and *rfp* reverse primer 5'-AGACTCGAGTTTGACAGCTCGTCCATGCC-3'. These genes contain BamHI and XhoI restriction sites. The SARS-CoV-2 M^{Pro} recombinant protein expression vector is derived from Shanghai variant and that was used to be amplified

by PCR for the cell expression with the following primers. The SARS-CoV-2 M^{Pro} gene, a forward primer 5'-ACCGGCG CGCCAAAGCTTACCATGCACCACCATCACCACCACGG CC-3' and a reverse primer 5'- TTGGATCCGGGCCCGGGG TTGGACTCAACGTCTCCTGCCAACTTGA GCAAATC AAAGTTTTGAAAGGTCACACCGCTGCACTG-3' with the AscHindIII and BamHI restriction sites. The reverse primer of M^{Pro} can encode F2A enhancing fusion with fluorescent proteins.

To detect SARS-CoV-2 M^{Pro} in cell lysates, 5×10^4 HEK-293T cells are seeded in 24-well plate and incubated at 5 % CO₂, 37 °C overnight. 10 % FBS DMEM medium is changed to DMEM without serum 4 h before transfection. Cells are then transfected with 0.5 μ g pcDNA3.1 M^{Pro}-CFP-YFP plasmid for continuous 4 h, using 2 μ l jetPRIME reagent (Cat no 712–60, Polyplus-transfection) per well. The cells are treated with 50 μ M and 100 μ M TFQ for 18 h posttransfection. The cell is washed with PBS well to discard medium in wells. 1X passive lysis buffer is added and cell lysate is shaken for 15 min, which homogenized cells for FRET measurement. Fluorescence of cell lysates is measured in the black plate, using multimode microplate reader (SpectraMax iD3, Molecular Device, CA95134) with excitation at 440 nm (± 10) and emission at 474 nm, 485 nm, and 528 nm. The untransfected cells are control without treatment. An average FRET intensity of transfected cells was obtained and compared with untransfected cells.

For immunofluorescence assay, 1×10^5 mock and stable clone M^{Pro}-GFP-RFP expression cells per well were seeded on coverslips, which were placed in 24-well plate, incubated at 37 °C, 5 % CO₂ overnight. The stable cells then were treated with 100 μ M TFQ and 50 μ M TFQ for 8 h. Following the immunofluorescence assay, cells were fixed with 4 % formalin for 30 min and were stained with DAPI, 20 min. Cells then were washed with PBS 3 times, for 5 min each washing. The mount solution was used to mount cells overnight at room temperature. This assay is performed in the dark.

TMPRSS2 activity in vivo

VeroE6-TMPRSS2 cells were seeded in a black, 96-well plate (5000 cells/well). Next day, the growth medium was replaced with 80 μ l of inhibitors (TFQ or compound 7) or PBS alone to the wells in the indicated concentrations (0.4 μ M, 2 μ M, and 10 μ M) and incubated at room temperature for 30 min. The fluorogenic substrate Boc-QAR-AMC (R&D Biosystems) was then added to each well to different concentrations (0, 1.5625 μ M, 3.125 μ M, 6.25 μ M, 12.5 μ M, 25 μ M, 50 μ M, and 100 μ M). Fluorescence (excitation 365 nm, emission 410 nm) was kinetically measured every 15 min for a total time of 150 min at 37 °C using Synergy H1 hybrid multimode microplate reader (BioTek Instruments, Inc). The Ki value was calculated by use of the competitive inhibition model in Graphpad Prism software.

Time course assay of TFQ

Vero E6 (7×10^4) cells were seeded in 24-well plates and subjected to two modes of drug treatment, one in which cells

were pretreated with drugs for an hour prior to viral infection, and the other without drug pretreatment. Cells were then infected with virus for 1 h in the absence of drugs. After infection, cells were washed with PBS and cultured with drug-containing medium until the end of the experiment. The virus-containing supernatants were harvested at 1 to 3 days post-infection and subjected to qRT-PCR to determine the viral titers. The viral cytopathic effect (CPE) was observed under microscope and imaged at 3 days post infection.

Viral RNA extraction and quantitative RT-PCR

The viral RNA in supernatant was extracted using the QIAamp Viral RNA Mini Kit (QIAGEN). The extracted RNA was reverse transcribed using SuperScript™ III reverse transcriptase (Invitrogen). The cDNAs were amplified by real-time PCR using the LightCycler FastStart DNA Master HybProbe (Roche Molecular Biochemicals) with a Light Cycler 96 (Roche Molecular Biochemicals) for 50 cycles of 10 s at 95 °C, annealing of 10 s at 58 °C, and elongation of 10 s at 72 °C to detect N gene of SARS-CoV2. The following primers and probe were used:

N_Sarbeco_F1:5'-CACATTGGCACCCGCAATC-3'
 N_Sarbeco_R1:5'-GAGGAACGAGAAGAGGCTTG-3'
 N_Sarbeco_P1: 5'-FAM- ACTTCCTCAAGGAACAA-CATTGCCA -BHQ1-3'.

Statistical analysis

Data of bar or curve graphs display as percentage or number compared with control groups with a standard deviation of two or three independent experiments. Microsoft Excel was used for statistical analyses. The two-tailed independent Student's *t* test was used to compare continuous variables between two groups. All experiments were carried out at least twice. The statistical significance with *p* value smaller than 0.05, 0.01, and 0.001 is indicated by *, ** and ***, respectively.

Data availability

The coordinates and structure factors of SARS-CoV-2 M^{pro}-Tafenoquine complex have been deposited in the Protein Data Bank with accession code 7DDC. All data are presented in the paper or the Supplementary Information. The materials used in this study should be requested from M.-C. H.

Supporting information—This article contains supporting information.

Acknowledgments—We would like to thank Ms Yi-Jen Liau at National Taiwan University for technical assistance of SARS-CoV-2 preparation, SCI Pharmtech Inc for providing HCQ, and Dr Jeng Cheng for professional editing and proofreading.

Author contributions—Y. C., W.-H. Y., H.-F. C., and J.-Y. G. conceptualization; Y. C., W.-H. Y., H.-F. C., J.-Y. G., Y.-C. W., L.-M. H., C.-S. Y., Y.-L. L., J.-S. C., Y.-P. C., D.-Y. C., L.-B. J., and C.-H. T. data curation; Y.-C. W., L.-M. H., C.-S. Y., Y.-L. L., J.-S. C., Y.-P. C., D.-Y. C., L.-B. J., and C.-H. T. formal analysis; Y. C., W.-H. Y., H.-F.

C., J.-Y. G., Y.-C. W., L.-M. H., C.-S. Y., Y.-L. L., M.-H. H., C.-L. T., Y.-Z. C., B.-Y. H., C.-F. H., Y.-L. H., Y.-P. C., W.-J. W., W.-C. S., V. K., Y.-C. W., S.-W. C., and C.-S. C. investigation; M.-C. H. project administration; Y. C., W.-H. Y., H.-F. C., and J.-Y. G. writing—original draft; M.-C. H. writing—review and editing.

Funding and additional information—This research was supported in part by the following: The Ministry of Science and Technology, Taiwan (MOST108-2311-B-241-001; to Y. C., MOST109-2327-B-039-003; to M.-C. H. and MOST110-2923-B-039-001-MY3; to C.-W. L.); Yingsai Young Scholar Award (CMU108-YTY-04; to W.-H. Y.); the “Drug Development Center, China Medical University” from the Featured Areas Research Center Program within the Framework of the Higher Education Sprout Project by the Ministry of Education (MOE), Taiwan.

Conflict of interest—The authors declare that there is no conflict of interests with the contents of this article.

Abbreviations—The abbreviations used are: AUC, analytical ultracentrifugation; CD, circular dichroism; CPE, cytopathic effect; DMEM, Dulbecco's modified eagle's medium; DSF, differential scanning fluorimetry; FBS, fetal bovine serum; FDA, Food and Drug Administration; FRET, fluorescence resonance energy transfer; MOI, multiplicity of infection; Orf, open reading frame; SARS-CoV-2, severe acute respiratory syndrome coronavirus 2; TFQ, tafenoquine; TMPRSS2, TFQ inhibited human transmembrane protease serine 2; Vpp, viral pseudoparticle.

References

- Zhu, N., Zhang, D., Wang, W., Li, X., Yang, B., Song, J., Zhao, X., Huang, B., Shi, W., Lu, R., Niu, P., Zhan, F., Ma, X., Wang, D., Xu, W., *et al.* (2020) A novel coronavirus from patients with pneumonia in China, 2019. *N. Engl. J. Med.* **382**, 727–733
- Zhou, P., Yang, X. L., Wang, X. G., Hu, B., Zhang, L., Zhang, W., Si, H. R., Zhu, Y., Li, B., Huang, C. L., Chen, H. D., Chen, J., Luo, Y., Guo, H., Jiang, R. D., *et al.* (2020) A pneumonia outbreak associated with a new coronavirus of probable bat origin. *Nature* **579**, 270–273
- Wu, F., Zhao, S., Yu, B., Chen, Y. M., Wang, W., Song, Z. G., Hu, Y., Tao, Z. W., Tian, J. H., Pei, Y. Y., Yuan, M. L., Zhang, Y. L., Dai, F. H., Liu, Y., Wang, Q. M., *et al.* (2020) A new coronavirus associated with human respiratory disease in China. *Nature* **579**, 265–269
- Dong, E., Du, H., and Gardner, L. (2020) An interactive web-based dashboard to track COVID-19 in real time. *Lancet Infect. Dis.* **20**, 533–534
- World Health Organization (2021) *Coronavirus Disease (COVID-19) Weekly Epidemiological Update and Weekly Operational Update*. World Health Organization, Geneva
- Pawlowski, C., Lenehan, P., Puranik, A., Agarwal, V., Venkatakrishnan, A. J., Niesen, M. J. M., O'Horo, J. C., Virk, A., Swift, M. D., Badley, A. D., Halamka, J., and Soundararajan, V. (2021) FDA-authorized COVID-19 vaccines are effective per real-world evidence synthesized across a multi-state health system. *Med. (N. Y.)* **2**, 979–992.e8
- Dagan, N., Barda, N., Kepten, E., Miron, O., Perchik, S., Katz, M. A., Hernán, M. A., Lipsitch, M., Reis, B., and Balicer, R. D. (2021) BNT162b2 mRNA covid-19 vaccine in a nationwide mass vaccination setting. *N. Engl. J. Med.* **384**, 1412–1423
- Levine-Tiefenbrun, M., Yelin, L., Katz, R., Herzog, E., Golan, Z., Schreiber, L., Wolf, T., Nadler, V., Ben-Tov, A., Kuint, J., Gazit, S., Patalon, T., Chodick, G., and Kishony, R. (2021) Initial report of decreased SARS-CoV-2 viral load after inoculation with the BNT162b2 vaccine. *Nat. Med.* **27**, 790–792
- Mathieu, E., Ritchie, H., Ortiz-Ospina, E., Roser, M., Hasell, J., Appel, C., Giattino, C., and Rodés-Guirao, L. (2021) A global database of COVID-19 vaccinations. *Nat. Hum. Behav.* **5**, 947–953

Inhibition of SARS-CoV-2 virus infection by tafenoquine and its derivatives

- Katz, I. T., Weintraub, R., Bekker, L. G., and Brandt, A. M. (2021) From vaccine nationalism to vaccine equity - finding a path forward. *N. Engl. J. Med.* **384**, 1281–1283
- Korber, B., Fischer, W. M., Gnanakaran, S., Yoon, H., Theiler, J., Abfalterer, W., Hengartner, N., Giorgi, E. E., Bhattacharya, T., Foley, B., Hastie, K. M., Parker, M. D., Partridge, D. G., Evans, C. M., Freeman, T. M., *et al.* (2020) Tracking changes in SARS-CoV-2 spike: Evidence that D614G increases infectivity of the COVID-19 virus. *Cell* **182**, 812–827. e19
- Reynolds, C. J., Pade, C., Gibbons, J. M., Butler, D. K., Otter, A. D., Menacho, K., Fontana, M., Smit, A., Sackville-West, J. E., Cutino-Moguel, T., Maini, M. K., Chain, B., Noursadeghi, M., UK COVIDsortium Immune Correlates Network, Brooks, T., *et al.* (2021) Prior SARS-CoV-2 infection rescues B and T cell responses to variants after first vaccine dose. *Science* **30**, eabh1282
- [preprint] Zahradník, J., Marciano, S., Shemesh, M., Zoler, E., Chiaravalli, J., Meyer, B., Rudich, Y., Dym, O., Elad, N., and Schreiber, G. (2021) SARS-CoV-2 RBD in vitro evolution follows contagious mutation spread, yet generates an able infection inhibitor. *bioRxiv*. <https://doi.org/10.1101/2021.01.06.425392>
- Wang, Z., Schmidt, F., Weisblum, Y., Muecksch, F., Barnes, C. O., Fink, S., Schaefer-Babajew, D., Cipolla, M., Gaebler, C., Lieberman, J. A., Oliveira, T. Y., Yang, Z., Abernathy, M. E., Huey-Tubman, K. E., Hurley, A., *et al.* (2021) mRNA vaccine-elicited antibodies to SARS-CoV-2 and circulating variants. *Nature* **592**, 616–622
- Collier, D. A., De Marco, A., Ferreira, I. A. T. M., Meng, B., Datir, R. P., Walls, A. C., Kemp, S. A., Bassi, J., Pinto, D., Silacci-Fregni, C., Bianchi, S., Tortorici, M. A., Bowen, J., Culap, K., Jaconi, S., *et al.* (2021) Sensitivity of SARS-CoV-2 B.1.1.7 to mRNA vaccine-elicited antibodies. *Nature* **593**, 136–141
- Vaidyanathan, G. (2021) Coronavirus variants are spreading in India - what scientists know so far. *Nature* **593**, 321–322
- Kumar, V., Singh, J., Hasnain, S. E., and Sundar, D. (2021) Possible link between higher transmissibility of B1617 and B117 variants of SARS-CoV-2 and increased structural stability of its spike protein and hACE2 affinity. *Int J. Mol. Sci.* **22**, 9131
- [preprint] Cherian, S., Potdar, V., Jadhav, S., Yadav, P., Gupta, N., Das, M., Das, S., Agarwal, A., Singh, S., Abraham, P., Panda, S., Mande, S., Swarup, R., Bhargava, B., Bhushan, R., *et al.* (2021) Convergent evolution of SARS-CoV-2 spike mutations, L452R, E484Q and P681R, in the second wave of COVID-19 in Maharashtra, India. *bioRxiv*. <https://doi.org/10.1101/2021.04.22.440932>
- [preprint] Tada, T., Zhou, H., Dcosta, B. M., Samanovic, M. I., Mulligan, M. J., and Landau, N. R. (2021) The spike proteins of SARS-CoV-2 B.1.617 and B.1.618 variants identified in India provide partial resistance to vaccine-elicited and therapeutic monoclonal antibodies. *bioRxiv*. <https://doi.org/10.1101/2021.05.14.444076>
- Chi, X., Yan, R., Zhang, J., Zhang, G., Zhang, Y., Hao, M., Zhang, Z., Fan, P., Dong, Y., Yang, Y., Chen, Z., Guo, Y., Zhang, J., Li, Y., Song, X., *et al.* (2020) A neutralizing human antibody binds to the N-terminal domain of the spike protein of SARS-CoV-2. *Science* **369**, 650–655
- Muik, A., Wallisch, A. K., Sängler, B., Swanson, K. A., Mühl, J., Chen, W., Cai, H., Maurus, D., Sarkar, R., Türeci, Ö., Dormitzer, P. R., and Şahin, U. (2021) Neutralization of SARS-CoV-2 lineage B.1.1.7 pseudovirus by BNT162b2 vaccine-elicited human sera. *Science* **371**, 1152–1153
- Wang, P., Nair, M. S., Liu, L., Iketani, S., Luo, Y., Guo, Y., Wang, M., Yu, J., Zhang, B., Kwong, P. D., Graham, B. S., Mascola, J. R., Chang, J. Y., Yin, M. T., Sobieszczyk, M., *et al.* (2021) Antibody resistance of SARS-CoV-2 variants B.1.351 and B.1.1.7. *Nature* **593**, 130–135
- Spinner, C. D., Gottlieb, R. L., Criner, G. J., Arribas López, J. R., Cattelan, A. M., Soriano Viladomiu, A., Ogbuagu, O., Malhotra, P., Mullane, K. M., Castagna, A., Chai, L. Y. A., Roestenberg, M., Tsang, O. T. Y., Bernasconi, E., Le Turnier, P., *et al.* (2020) Effect of Remdesivir versus standard care on clinical status at 11 days in patients with moderate COVID-19: A randomized clinical trial. *JAMA* **324**, 1048–1057
- Wang, Y., Zhang, D., Du, G., Du, R., Zhao, J., Jin, Y., Fu, S., Gao, L., Cheng, Z., Lu, Q., Hu, Y., Luo, G., Wang, K., Lu, Y., Li, H., *et al.* (2020) Remdesivir in adults with severe COVID-19: A randomised, double-blind, placebo-controlled, multicentre trial. *Lancet* **395**, 1569–1578
- Group, R. C., Horby, P., Lim, W. S., Emberson, J. R., Mafham, M., Bell, J. L., Linsell, L., Staplin, N., Brightling, C., Ustianowski, A., Elmahi, E., Prudon, B., Green, C., Felton, T., Chadwick, D., *et al.* (2021) Dexamethasone in hospitalized patients with Covid-19. *N. Engl. J. Med.* **384**, 693–704
- Jirjees, F., Saad, A. K., Al Hano, Z., Hatahet, T., Al Obaidi, H., and Dallal Bashi, Y. H. (2021) COVID-19 treatment guidelines: Do they really reflect best medical practices to manage the pandemic? *Infect. Dis. Rep.* **13**, 259–284
- Taylor, P. C., Adams, A. C., Hufford, M. M., de la Torre, I., Winthrop, K., and Gottlieb, R. L. (2021) Neutralizing monoclonal antibodies for treatment of COVID-19. *Nat. Rev. Immunol.* **21**, 382–393
- WHO Solidarity Trial Consortium, Pan, H., Peto, R., Henao-Restrepo, A. M., Preziosi, M. P., Sathiyamoorthy, V., Abdool Karim, Q., Alejandria, M. M., Hernández García, C., Kieny, M. P., Malekzadeh, R., Murthy, S., Reddy, K. S., Roses Periago, M., Abi Hanna, P., *et al.* (2021) Repurposed antiviral drugs for Covid-19 - interim WHO solidarity trial results. *N. Engl. J. Med.* **384**, 497–511
- Lee, T. C., McDonald, E. G., Butler-Laporte, G., Harrison, L. B., Cheng, M. P., and Brophy, J. M. (2021) Remdesivir and systemic corticosteroids for the treatment of COVID-19: A Bayesian re-analysis. *Int. J. Infect. Dis.* **104**, 671–676
- Naqvi, A. A. T., Fatima, K., Mohammad, T., Fatima, U., Singh, I. K., Singh, A., Atif, S. M., Hariprasad, G., Hasan, G. M., and Hassan, M. I. (2020) Insights into SARS-CoV-2 genome, structure, evolution, pathogenesis and therapies: Structural genomics approach. *Biochim. Biophys. Acta Mol. Basis Dis.* **1866**, 165878
- Pillaiyar, T., Manickam, M., Namasivayam, V., Hayashi, Y., and Jung, S. H. (2016) An overview of severe acute respiratory syndrome-coronavirus (SARS-CoV) 3CL protease inhibitors: Peptidomimetics and small molecule chemotherapy. *J. Med. Chem.* **59**, 6595–6628
- Anand, K., Ziebuhr, J., Wadhwani, P., Mesters, J. R., and Hilgenfeld, R. (2003) Coronavirus main proteinase (3CLpro) structure: Basis for design of anti-SARS drugs. *Science* **300**, 1763–1767
- Hegyí, A., and Ziebuhr, J. (2002) Conservation of substrate specificities among coronavirus main proteases. *J. Gen. Virol.* **83**, 595–599
- Gordon, D. E., Jang, G. M., Bouhaddou, M., Xu, J., Obernier, K., White, K. M., O'Meara, M. J., Rezelj, V. V., Guo, J. Z., Swaney, D. L., Tummino, T. A., Hüttenhain, R., Kaake, R. M., Richards, A. L., Tutuncuoglu, B., *et al.* (2020) A SARS-CoV-2 protein interaction map reveals targets for drug repurposing. *Nature* **583**, 459–468
- Hoffmann, M., Kleine-Weber, H., Schroeder, S., Krüger, N., Herrler, T., Erichsen, S., Schiergens, T. S., Herrler, G., Wu, N. H., Nitsche, A., Müller, M. A., Drosten, C., and Pöhlmann, S. (2020) SARS-CoV-2 cell entry depends on ACE2 and TMPRSS2 and is blocked by a clinically proven protease inhibitor. *Cell* **181**, 271–280.e8
- Wang, Y. C., Yang, W. H., Yang, C. S., Hou, M. H., Tsai, C. L., Chou, Y. Z., Hung, M. C., and Chen, Y. (2020) Structural basis of SARS-CoV-2 main protease inhibition by a broad-spectrum anti-coronaviral drug. *Am. J. Cancer Res.* **10**, 2535–2545
- Campo, B., Vandal, O., Wesche, D. L., and Burrows, J. N. (2015) Killing the hypnozoite—drug discovery approaches to prevent relapse in Plasmodium vivax. *Pathog. Glob. Health* **109**, 107–122
- Ebstie, Y. A., Abay, S. M., Tadesse, W. T., and Ejigu, D. A. (2016) Tafenoquine and its potential in the treatment and relapse prevention of Plasmodium vivax malaria: The evidence to date. *Drug Des. Devel. Ther.* **10**, 2387–2399
- Frampton, J. E. (2018) Tafenoquine: First global approval. *Drugs* **78**, 1517–1523
- Hounkpatin, A. B., Kreidenweiss, A., and Held, J. (2019) Clinical utility of tafenoquine in the prevention of relapse of Plasmodium vivax malaria: A review on the mode of action and emerging trial data. *Infect. Drug Resist.* **12**, 553–570
- Liu, J., Cao, R., Xu, M., Wang, X., Zhang, H., Hu, H., Li, Y., Hu, Z., Zhong, W., and Wang, M. (2020) Hydroxychloroquine, a less toxic

- derivative of chloroquine, is effective in inhibiting SARS-CoV-2 infection *in vitro*. *Cell Discov.* **6**, 16
42. Bansal, P., Goyal, A., Cusick, A., Lahan, S., Dhaliwal, H. S., Bhyani, P., Bhattad, P. B., Aslam, F., Ranka, S., Dalia, T., Chhabra, L., Sanghavi, D., Sonani, B., and Davis, J. M. (2021) Hydroxychloroquine: A comprehensive review and its controversial role in coronavirus disease 2019. *Ann. Med.* **53**, 117–134
 43. Mitjà, O., Corbacho-Monné, M., Ubals, M., Alemany, A., Suñer, C., Tebé, C., Tobias, A., Peñafiel, J., Ballana, E., Pérez, C. A., Admella, P., Riera-Martí, N., Laporte, P., Mitjà, J., Clua, M., *et al.* (2021) A cluster-randomized trial of hydroxychloroquine for prevention of Covid-19. *N. Engl. J. Med.* **384**, 417–427
 44. Ayerbe, L., Risco-Risco, C., Núñez-Gil, I., Perez-Piñar, M., and Ayis, S. (2021) Hydroxychloroquine treatment does not reduce COVID-19 mortality; underdosing to the wrong patients? *Lancet Rheumatol.* **3**, e172
 45. Pantoliano, M. W., Petrella, E. C., Kwasnoski, J. D., Lobanov, V. S., Myslik, J., Graf, E., Carver, T., Asel, E., Springer, B. A., Lane, P., and Saleme, F. R. (2001) High-density miniaturized thermal shift assays as a general strategy for drug discovery. *J. Biomol. Screen.* **6**, 429–440
 46. Seetoh, W. G., and Abell, C. (2016) Disrupting the constitutive, homodimeric protein-protein interface in CK2 β using a biophysical fragment-based approach. *J. Am. Chem. Soc.* **138**, 14303–14311
 47. Woolger, N., Bournazos, A., Sophocleous, R. A., Evesson, F. J., Lek, A., Driemer, B., Sutton, R. B., and Cooper, S. T. (2017) Limited proteolysis as a tool to probe the tertiary conformation of dysferlin and structural consequences of patient missense variant L344P. *J. Biol. Chem.* **292**, 18577–18591
 48. Jin, Z., Du, X., Xu, Y., Deng, Y., Liu, M., Zhao, Y., Zhang, B., Li, X., Zhang, L., Peng, C., Duan, Y., Yu, J., Wang, L., Yang, K., Liu, F., *et al.* (2020) Structure of M(pro) from SARS-CoV-2 and discovery of its inhibitors. *Nature* **582**, 289–293
 49. Hoffmann, M., Hofmann-Winkler, H., Krüger, N., Kempf, A., Nehlmeier, I., Graichen, L., Arora, P., Sidarovich, A., Moldenhauer, A. S., Winkler, M. S., Schulz, S., Jäck, H. M., Stankov, M. V., Behrens, G. M. N., and Pöhlmann, S. (2021) SARS-CoV-2 variant B.1.617 is resistant to bamlanivimab and evades antibodies induced by infection and vaccination. *Cell Rep.* **36**, 109415
 50. Park, W. B., Kwon, N. J., Choi, S. J., Kang, C. K., Choe, P. G., Kim, J. Y., Yun, J., Lee, G. W., Seong, M. W., Kim, N. J., Seo, J. S., and Oh, M. D. (2020) Virus isolation from the first patient with SARS-CoV-2 in Korea. *J. Korean Med. Sci.* **35**, e84
 51. Vicenzi, E., Canducci, F., Pinna, D., Mancini, N., Carletti, S., Lazzarin, A., Bordignon, C., Poli, G., and Clementi, M. (2004) Coronaviridae and SARS-associated coronavirus strain HSR1. *Emerg. Infect. Dis.* **10**, 413–418
 52. Yan, H., Xiao, G., Zhang, J., Hu, Y., Yuan, F., Cole, D. K., Zheng, C., and Gao, G. F. (2004) SARS coronavirus induces apoptosis in vero E6 cells. *J. Med. Virol.* **73**, 323–331
 53. Harcourt, J., Tamin, A., Lu, X., Kamili, S., Sakthivel, S. K., Murray, J., Queen, K., Tao, Y., Paden, C. R., Zhang, J., Li, Y., Uehara, A., Wang, H., Goldsmith, C., Bullock, H. A., *et al.* (2020) Severe acute respiratory syndrome coronavirus 2 from patient with coronavirus disease, United States. *Emerg. Infect. Dis.* **26**, 1266–1273
 54. Ragia, G., and Manolopoulos, V. G. (2020) Inhibition of SARS-CoV-2 entry through the ACE2/TMPRSS2 pathway: A promising approach for uncovering early COVID-19 drug therapies. *Eur. J. Clin. Pharmacol.* **76**, 1623–1630
 55. Xiu, S., Dick, A., Ju, H., Mirzaie, S., Abdi, F., Cocklin, S., Zhan, P., and Liu, X. (2020) Inhibitors of SARS-CoV-2 entry: Current and future opportunities. *J. Med. Chem.* **63**, 12256–12274
 56. Mahmoud, I. S., Jarrar, Y. B., Alshaer, W., and Ismail, S. (2020) SARS-CoV-2 entry in host cells-multiple targets for treatment and prevention. *Biochimie* **175**, 93–98
 57. Hoffmann, M., Mösbauer, K., Hofmann-Winkler, H., Kaul, A., Kleine-Weber, H., Krüger, N., Gassen, N. C., Müller, M. A., Drosten, C., and Pöhlmann, S. (2020) Chloroquine does not inhibit infection of human lung cells with SARS-CoV-2. *Nature* **585**, 588–590
 58. Yang, H., Yang, M., Ding, Y., Liu, Y., Lou, Z., Zhou, Z., Sun, L., Mo, L., Ye, S., Pang, H., Gao, G. F., Anand, K., Bartlam, M., Hilgenfeld, R., and Rao, Z. (2003) The crystal structures of severe acute respiratory syndrome virus main protease and its complex with an inhibitor. *Proc. Natl. Acad. Sci. U. S. A.* **100**, 13190–13195
 59. Verschuere, K. H., Pumpor, K., Anemüller, S., Chen, S., Mesters, J. R., and Hilgenfeld, R. (2008) A structural view of the inactivation of the SARS coronavirus main proteinase by benzotriazole esters. *Chem. Biol.* **15**, 597–606
 60. [preprint] Fornasier, E., Macchia, M. L., Giachin, G., Susic, A., Pavan, M., Sturlese, M., Salata, C., Moro, S., Gatto, B., Bellanda, M., and Battistutta, R. (2021) A novel conformational state for SARS-CoV-2 main protease. *bioRxiv*. <https://doi.org/10.1101/2021.03.04.433882>
 61. Lockbaum, G. J., Reyes, A. C., Lee, J. M., Tilwawala, R., Nalivaika, E. A., Ali, A., Kurt Yilmaz, N., Thompson, P. R., and Schiffer, C. A. (2021) Crystal structure of SARS-CoV-2 main protease in complex with the non-covalent inhibitor ML188. *Viruses* **13**, 174
 62. Günther, S., Reinke, P. Y. A., Fernández-García, Y., Lieske, J., Lane, T. J., Ginn, H. M., Koua, F. H. M., Ehrt, C., Ewert, W., Oberthuer, D., Yefanov, O., Meier, S., Lorenzen, K., Krichel, B., Kopicki, J. D., *et al.* (2021) X-ray screening identifies active site and allosteric inhibitors of SARS-CoV-2 main protease. *Science* **372**, 642–646
 63. [preprint] Su, H., Yao, S., Zhao, W., Li, M., Liu, J., Shang, W., Xie, H., Ke, C., Gao, M., Yu, K., Liu, H., Shen, J., Tang, W., Zhang, L., Zuo, J., *et al.* (2020) Discovery of baicalin and baicalein as novel, natural product inhibitors of SARS-CoV-2 3CL protease *in vitro*. *bioRxiv*. <https://doi.org/10.1101/2020.04.13.038687>
 64. Aljoundi, A., Bji, I., El Rashedy, A., and Soliman, M. E. S. (2020) Covalent versus non-covalent enzyme inhibition: Which route should we take? A justification of the good and bad from molecular modelling perspective. *Protein J.* **39**, 97–105
 65. Böttger, R., Hoffmann, R., and Knappe, D. (2017) Differential stability of therapeutic peptides with different proteolytic cleavage sites in blood, plasma and serum. *PLoS One* **12**, e0178943
 66. Haston, J. C., Hwang, J., and Tan, K. R. (2019) Guidance for using tafenoquine for prevention and antirelapse therapy for malaria - United States, 2019. *MMWR Morb. Mortal. Wkly Rep.* **68**, 1062–1068
 67. Hossain, M. K., Hassanzadeganroudsari, M., Feehan, J., and Apostolopoulos, V. (2021) The emergence of new strains of SARS-CoV-2. What does it mean for COVID-19 vaccines? *Expert Rev. Vaccines* **20**, 635–638
 68. Singh, J., Singh, J., Rahman, S. A., Ehtesham, N. Z., Hira, S., and Hasnain, S. E. (2021) SARS-CoV-2 variants of concern are emerging in India. *Nat. Med.* **27**, 1131–1133
 69. Lo, M. C., Aulabaugh, A., Jin, G., Cowling, R., Bard, J., Malamas, M., and Ellestad, G. (2004) Evaluation of fluorescence-based thermal shift assays for hit identification in drug discovery. *Anal. Biochem.* **332**, 153–159
 70. Schuck, P., Perugini, M. A., Gonzales, N. R., Howlett, G. J., and Schubert, D. (2002) Size-distribution analysis of proteins by analytical ultracentrifugation: Strategies and application to model systems. *Biophys. J.* **82**, 1096–1111